

pubs.acs.org/cm Article

Depth-Dependent Understanding of Cathode Electrolyte Interphase (CEI) on the Layered Li-Ion Cathodes Operated at Extreme High Temperature

Sudhan Nagarajan, Conan Weiland, Sooyeon Hwang, Mahalingam Balasubramanian, and Leela Mohana Reddy Arava*



Cite This: Chem. Mater. 2022, 34, 4587–4601



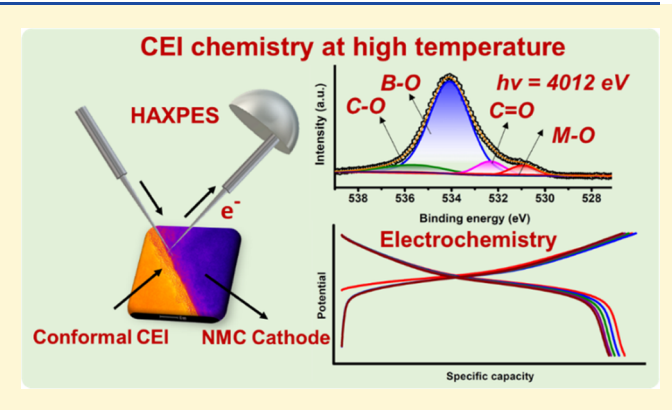
ACCESS

III Metrics & More

Article Recommendations

Supporting Information

ABSTRACT: The high-temperature operation of Li-ion batteries is highly dependent on the stability of the cathode electrolyte interphase (CEI) formed during lithiation—delithiation reactions. However, knowledge on the nature of the CEI is limited and its stability under extreme temperatures is not well understood. Therefore, herein, we investigate a proof-of-concept study on stabilizing CEI on model LiNi_{0.33}Mn_{0.33}Co_{0.33}O₂ (NMC333) at an extreme operation condition of 100 °C using the thermally stable pyrrolidinium-based ionic liquid electrolyte. The electrochemical lithiation—delithiation reactions at 100 °C and the CEI evolution upon different cycling conditions are investigated. Further, the depth-dependent CEI chemistry was investigated using energy-tunable synchrotron-based hard X-ray photoelectron spectroscopy (HAXPES). The results reveal that the high-temperature operation



accelerated the CEI formation compared to room temperature, and the surface of the interphase layer is rich in boron-based inorganic moieties than the deeper surface. Further, bulk-sensitive X-ray absorption spectroscopy (XAS) was used to investigate the transition-metal redox contributors during high-temperature electrochemical reactions; similar to room temperature, the Ni^{2+/4+} redox couple is the only charge-compensating redox couple during high-temperature operation. Finally, the physical nature of the conformal CEI on the cathode particles was visualized with high-resolution transmission electron microscopy, which confirms that the significant degradation of cathode particles without conformal CEI is due to the transformation of a layer-to-spinel formation at extreme temperature. In this study, understanding this high-temperature interfacial chemistry of NMC cathodes through advanced spectroscopy and microscopy will shed light on transforming the ambient-temperature Li-ion chemistry into high-temperature applications.

■ INTRODUCTION

Rechargeable Li-ion batteries are key components of portable electronics, and the current process of electrifying gasoline vehicles to electric vehicles strongly relies on the advancement in the current Li-ion batteries. 1,2 The demand for Li-ion batteries is steadily growing, and zero-carbon goals for achieving a safe and sustainable society have led to intensive research on developing high-performance battery materials. With the current Li-ion technology, the batteries can be safely operated between room temperature (RT) to 60 °C, and operation beyond this suggested temperature range will lead to irreversible degradation often resulting in low cell capacity, cycle life, and sometimes catastrophic failures such as fires and explosions.³⁻⁶ However, there are a number of industrial applications that require high-performance rechargeable batteries operated in aggressive environments. These applications include military applications, sensor applications, and oil and gas industry drilling applications.3 To date, Li-ion primary

battery based on Li-SOCl₂ chemistry is one of the major contenders in the high-temperature (HT) battery applications, which can be operated up to 150 °C.⁷ However, the high-temperature-compatible batteries are mostly primary batteries that require periodic replacement after being completely discharged. Moreover, this constant care during operation leads to significant maintenance tasks and environmental impact of spent electronic battery material waste. In recent days, the demand for high-temperature rechargeable battery chemistries that are specifically suitable for the oil and gas

Received: February 10, 2022 Revised: April 8, 2022 Published: May 3, 2022





industry is growing.⁶ Therefore, high-temperature-compatible Li-ion batteries are promising alternative solutions that will potentially replace the high-temperature primary battery technologies for many industrial applications.⁶ To date, several research groups have investigated the high-temperature compatibility of Li-ion rechargeable batteries using functional electrolyte additives, solvent engineering, and electrolyte design strategies.^{8–11} However, the intrinsic physicochemical properties such as flammability, high volatility, thermal stability, low flash point, and melting temperature restrict the implementation of carbonate electrolytes to explore current battery materials at extreme-temperature applications. 12,13 Therefore, an alternative to flammable organic liquid electrolytes, another electrolyte chemistry with enhanced thermal stability is room-temperature ionic liquids (RTILs), and there have been various investigations of exploring RTILs for the extreme-temperature operation of current Li-ion batteries. 14,15

In general, RTILs are excellent candidates that possess superior physicochemical properties such as nonvolatility, nonflammability, a wide liquidus range, and high conductivity, which made RTIL one of the important solvents for rechargeable batteries. To date, various Li-ion battery electrode materials such as $\text{Li}_4\text{Ti}_5\text{O}_{12}$, graphite, metallic lithium anodes, and cathodes such as LiFePO_4 , LiCoO_2 , $\text{Li}_1(\text{Ni}_3,\text{Mn}_3,\text{Co}_3)$, and $\text{LiNi}_{0.5}\text{Mn}_{1.5}\text{O}_4$ were investigated previously by many research groups including our own published works. The superior of the properties of the

Among various cathode materials, the NMC-based layered cathodes are potential electrode materials due to their high energy density and high cycle life. More importantly, the performance of the electrode materials is strongly dependent on the electrolyte formulation and the electrode/electrolyte interface is the key to stabilize the reactive cathode materials from the electrolyte at high-temperature lithiation and delithiation reactions. $^{22-24}$ To mitigate the electrode/electrolyte interfacial issues, the reactive electrode surface with functional interface coating during synthesis and modifying electrolyte formulation for attaining in situ-formed cathode electrolyte interphase (CEI) films have been studied previously.²⁴⁻²⁷ Among these strategies, the in situ-formed cathode electrolyte interface on the reactive cathode surface by functional additives is found to be a successful strategy compared to the coating of the cathode surface during its synthesis. ^{28–30} With this significance, identifying and understanding a nanoscale electrode/electrolyte interface layer, especially cathode electrolyte interphase evolution during high-temperature cycling, are of paramount importance to transform ambient-temperature technology to high-temperature applications.

Hence, we hypothesize that a thermally stable cathode electrolyte interface layer will improve extreme-temperature performance by preventing the reactive cathode materials from direct contact with electrolytes and further structural degradation. Therefore, the identification of thermally stable interphase layer formation and understanding its chemical constituents at buried interfaces are the key strategies to explore high-temperature compatibility of cathode materials. High-temperature performance and thermal stability of the cathode materials are linked to elemental composition, functional groups, and bonding environments on the cathode surface at different depth levels. Understanding the complex interfacial chemistry of battery materials, the synchrotron-based hard X-ray photoelectron spectroscopy technique is a

suitable method due to its nondestructive variable depth probing capability and energy tunability for probing surface and buried interfaces without destructing the local bonding environment. The continuous lithiation and delithiation reactions at high temperature are highly dependent on the parasitic reactions occurring at the electrode/electrolyte interfaces. Therefore, the redox couple contribution toward observed specific capacity at high-temperature lithiation and delithiation reactions could be tracked by bulk-sensitive hard X-ray absorption spectroscopy (XAS) technique, which enables local bonding environment and redox couple evolutions to be identified in the bulk of the material.

In this study, we attempted to investigate the electrode/ electrolyte interface formed on the model NMC333 cathode operated in thermally stable ionic liquid environments with thermally stable cathode electrolyte interphase. In this work, the reversible lithiation and delithiation reactions were performed in the model NMC cathode composition at an extreme high-temperature operation of 100 °C. Further, the detailed redox contribution toward the observed capacity at high-temperature operation was investigated using bulksensitive hard X-ray absorption spectroscopy. Furthermore, the depth-dependent high-temperature-compatible electrode/ electrolyte interphase chemistry was understood with hard Xray photoelectron spectroscopy (HAXPES), and the nature of the cathode electrolyte interphase (CEI) was investigated with high-resolution transmission electron microscopy. Overall, this fundamental hypothesis-driven interfacial chemistry research dealt with advanced spectroscopy and microscopy approaches in understanding high-temperature cathode material research and further developing high-temperature battery technology for many demanding industrial applications.

■ EXPERIMENTAL SECTION

Materials. Bis(trifluoromethane sulfonamide) lithium salt (LiTF-SI; 99.95%) and lithium difluoro(oxalato) borate (LiDFOB) were purchased from Sigma-Aldrich. Fluoroethylene carbonate (FEC; 98%) solvent was purchased from Alfa Aesar. Ionic liquid electrolyte was prepared by dissolving an appropriate amount of LiTFSI in 1-butyl 1-methylpyrrolidinium bis trifluoromethane sulfonimide (Py14TFSI)(Iolitec; 99%) ionic liquid solvent. In this electrolyte mixture, an appropriate amount of LiDFOB salt and FEC solvent additives was added at room temperature. Prior to electrolyte preparation, the ionic liquid was dried at 100 °C under vacuum conditions. All of the above electrolyte preparations were carried out inside a glovebox circulated with a high purity Ar gas (<1 ppm $\rm O_2$ and <0.1 $\rm H_2O$).

Electrochemical Characterization. All of the electrode preparation was performed in an argon-filled glovebox. All of the electrodes were prepared by the slurry coating method. The electrode slurry was prepared by mixing active material, conductive carbon (C65, MTI), and poly(vinylidene difluoride) (PVDF) binder (Sigma-Aldrich) in a ratio of 85:10:5 using N-methyl-2-pyrrolidone (NMP) as a solvent (Sigma-Aldrich). The homogeneous mixture was cast on an aluminum current collector (15 μ m thickness, MTI) using the Dr blade method. The coated electrodes were dried at 80 $^{\circ}\text{C}$ in a vacuum oven for at least 12 h. Finally, the electrodes were cut into circles and yielded a loading of 2-3 mg on each electrode. All electrochemical analyses were performed in high-temperature-compatible coin cells (CR 2032), and the cells were prepared in an Ar-filled glovebox (O₂ < 1 ppm, $H_2O < 0.1$ ppm). Li foil (0.75 mm, Alfa Aesar) was used as the anode and its surface was cleaned using razor blades; quartz membrane was used as a separator. All of the galvanostatic tests were tested on an Arbin battery cycler at either 10 or 30 mA/g current density. For high-temperature charge-discharge studies, the fabricated cells were connected in a high-temperature oven to maintain a

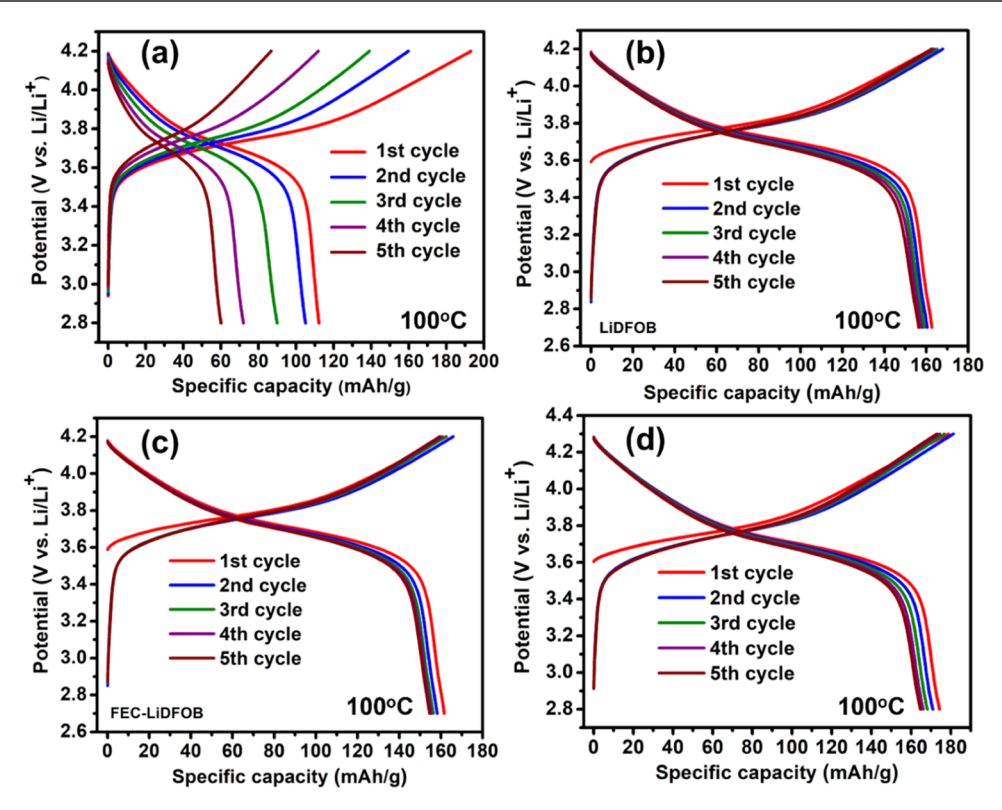


Figure 1. Electrochemical performance of the NMC333 cathode at 100 °C in ionic liquid electrolyte. (a) The galvanostatic charge—discharge profile of NMC333 at 100 °C in ionic liquid electrolyte without additives, (b) with additives at 2 wt % LiDFOB, (c) 2 wt % FEC and 2 wt % LiDFOB, and (d) cycled up to 4.3 V vs Li/Li⁺.

constant temperature of 100° C. Prior to high-temperature studies, the cells were cycled at room-temperature formation cycle for one complete charge—discharge cycle at 10 mA/g current density. The specific capacity was calculated for all electrodes based on the active material loading in the cathode. X-ray powder diffraction (XRD) was carried out on a Bruker D8 diffractometer using Cu K α radiation (1.54 Å) in the 2θ range from $10 \text{ to } 80^{\circ}$.

High-Resolution Transmission Electron Microscopy (HR-TEM). The HR-TEM measurements were performed at the Center for Functional Nanomaterials, Brookhaven National Laboratory. For all of the microscopy experiments, once the targeted electrodes attained the desired state of charge, the electrode materials were collected from the coated slurry on the Al current collector. The collected particles were sonicated in a vial with anhydrous dimethyl carbonate (DMC) to ensure uniform dispersion prior to drop-casting on a lacey carbon-coated TEM grid. Extreme care was taken to avoid air exposure to the samples, and the sample preparation was carried out in an Ar-filled glovebox. The bright-field HR-TEM and selected area electron diffraction (SAED) patterns were obtained with a Thermo-Fisher Talos F200X TEM instrument at an accelerating voltage of 200 kV. The TEM images were processed with digital micrograph (Gatan) software.

X-ray Absorption Spectroscopy (XAS). Ex situ XAS measurements were performed at the Advanced Photon Source beamline 20-BM-B at Argonne National Laboratory. The incident beam energy was monochromatized by a Si(111) crystal monochromator. The energy calibration was performed by simultaneously measuring corresponding metal foils such as Ni, Co, and Mn. The spectra were acquired in a transmission mode using gas ionization chamber as detectors. Once the coin cells attained their desired state of charge, the samples were collected from the coin cells and washed with DMC three times inside a glovebox. After complete drying, the collected electrodes were sandwiched between Kapton films and pasted on an appropriate beamline sample plate. The sealed samples were sent to beamline end station while completely avoiding air exposure. The Ni K edge, Co K edge, and Mn K edge data were processed (calibration,

energy alignment, and normalization) with the ATHENA software package.³¹ For all Ni, Co, and Mn K edge spectra, the energy calibration was carried out with the zero energy defined according to Kraft et al.³²

Hard X-ray Photoelectron Spectroscopy (HAXPES). The HAXPES measurements were performed at the National Institute of Standards and Technology beamline 7-ID-2 (SST-2) of National Synchrotron Light Source II of Brookhaven National Laboratory, using a 400 mm diameter concentric hemispherical analyzer oriented parallel to the photon polarization axis and perpendicular to the photon propagation axis. The HAXPES experiments were carried out in three different photon energies (2013, 4012, and 6508 eV). The 2013 eV photon energy selection was achieved using a double Si(111) crystal monochromator, while 4013 eV as well as 6508 eV photon energies were attained using a Si(220) monochromator. The lowenergy measurement was carried out with a pass energy of 50 eV, and the high-energy measurements (4012 and 6508 eV) used 200 eV pass energy. To avoid air exposure during sample preparation, once the cells achieved the required state of charge, the coin cells were disassembled inside the Ar-filled glovebox $(O_2 < 1 \text{ ppm, } H_2O < 0.1)$ ppm) and washed with anhydrous dimethyl carbonate to remove the electrolyte salt residue. Further, the electrode materials were pasted on a synchrotron sample bar using ultra-high-vacuum-compatible copper tape before being taken to the beamline end station. The sample bar was mounted to the analysis chamber using an inert sample transfer system, and samples were kept under ultra-high vacuum chamber overnight before starting the analysis. The raw data were processed with the CasaXPS software package. The presented binding energy scales for each sample in this study are referenced to C 1s spectra at 285 eV.

RESULTS AND DISCUSSION

Electrochemical Behavior of NMC at 100 °C. In this work, the NMC333 model compound was used to understand the electrode/electrolyte interfacial chemistry for developing

battery materials that are compatible in extreme environments. The high-temperature performance (100 °C) of the model NMC333 cathode was evaluated with and without surface filmforming agents, and a detailed electrochemical investigation is shown in Figure 1. Fundamentally, the objective of this study is to understand the extreme high-temperature performance of NMC333 cathodes in ionic liquid-based electrolytes that have negligible vapor pressure, but their ability to form stable CEI at high temperature is unknown. In this work, the NMC333 is used as a model cathode to evaluate the surface film formation ability and further its effect on electrochemical performance, interfacial stability, and structural stability at an extreme operating environment of 100 °C. For cathode electrolyte interphase, the lithium difluoro(oxalato)borate (LiDFOB) is chosen due to its use as a lithium salt additive in the carbonatebased electrolyte for forming CEI on oxide cathodes.³³ Fundamentally, the mechanism behind the additive chemistry is directly related to the highest occupied molecular orbital (HOMO) and lowest unoccupied molecular orbital (LUMO) levels of the additive compounds. This enables the additive compounds to be oxidized or reduced prior to the electrolyte solvent on the cathodes or anodes, respectively. Based on the theoretical calculations, the HOMO-LUMO levels of LiDFOB lie in the window of majority of the carbonate solvents; therefore, the LiDFOB salt preferentially oxidizes at the cathode during high voltage and reduces at the anode during low voltage, thereby forming a stable surface layer that prevents the further reaction between the electrodes and electrolytes.³⁴ Similarly, fluoroethylene carbonate (FEC) is a widely used reductive-based additive for forming passivation layers on the anode side to prevent further electrolyte reactions with the anodes at room temperature and elevated temperature.³⁵ Also, the FEC addition in the carbonate electrolyte is considered for cathodes and attracted interest due to its filmforming ability at the cathode side during electrochemical reactions. 36-38 With this understanding of functional additives, an in-depth understanding of the thermally stable cathode electrolyte interphase on the cathode surface is a key component, and its nanoscale evolution during electrochemical cycling determines the electrochemical lithiation and delithiation reactions at extreme temperature (100 °C). As shown in Figure 1, the NMC cathode was cycled against the metallic lithium anode in bis trifluoromethane sulfonimide lithium salt (LiTFSI) dissolved in the pyrrolidinium-based 1-butyl 1methyl pyrrolidinium bis trifluoromethane sulfonimide (Py14TFSI) ionic liquid electrolyte with or without filmforming additives. Figure 1a shows the charge-discharge profiles of the NMC333 cathode in 0.8 M LiTFSI in Pyr₁₄TFSI ionic liquid electrolyte at a high-temperature environment (100 °C). The first charge cycle exhibited a charge-specific capacity of more than 200 mAh/g, implying that the parasitic reactions are taking place at the electrode/electrolyte interface during high-temperature operation. Further, the chargedischarge profiles exhibited huge polarization and capacity fade as the cycle number continues, indicating that the cathode material is severely being degraded during high-temperature lithiation and delithiation reactions. More importantly, even though the voltage profiles are slopy similar to the conventional NMC333 cathode performance, 39 each charge-discharge cycle demonstrates huge capacity fade, which led to a complete degradation within five continuous charge-discharge cycles. Based on the previous works, this observed phenomenon could be attributed to the parasitic reaction-induced

structural degradation, implying that the cathode surface is significantly reactive with the electrolyte in an aggressive environment. 40 With this understanding, to prevent the direct contact between the cathode surface and electrolyte during the electrochemical reaction at 100 °C, it is hypothesized that having a stable nanoscale surface film on the cathode surface would improve the cathode interfacial stability, thereby achieving stable high-temperature lithiation-delithiation reactions. To prove this hypothesis, initially, 2 wt % lithium difluoro oxalate borate (LiDFOB) was added to the electrolyte and its charge-discharge profiles were tested in the upper voltage range of 4.2 V vs Li/Li⁺ at 100 °C. Interestingly, the addition of 2 wt % LiDFOB showed a significant improvement in the capacity fade and voltage polarization, indicating that the minimal quantity of LiDFOB played a significant role in protecting the reactive cathode surface by forming a thermally stable cathode electrolyte interphase film. As per Figure 1b, the NMC333 cathode with an electrolyte containing 2 wt % LiDFOB exhibited typical charge-discharge profiles and demonstrated stable lithiation-delithiation reactions at extremely high-temperature operation. Further, the capacity evolution at 100 °C was recorded for continuous chargedischarge cycles and is shown in Figure S2b. The LiDFOB salt solubility is not high because the addition of 3 wt % LiDFOB electrolyte was not successful as it seems to be nontransparent (Figure S4). With this solubility restriction, increasing the LiDFOB quantity for addressing the gradual capacity may not be a viable option. Therefore, we explored a holistic approach by adding one more high-temperature stable additive named fluoroethylene carbonate (FEC) into the previous LiDFOB electrolyte formulation, and the electrochemical performance was evaluated.

As shown in Figure 1c, by adding 2 wt % FEC, reversible lithiation and delithiation reactions of the NMC333 cathode were improved at high temperature and stable performance with a 96% Coulombic efficiency for about 30 continuous charge-discharge cycles was recorded (Figure S2c). Further, the upper cutoff was increased to 4.3 V vs Li/Li⁺ against the lithium metal, and the voltage profiles demonstrated stable lithiation-delithiation reactions with a specific capacity value of 175 mAh/g at 30 mA/g current density (Figure 1d). This observation confirms that a linear relationship in high lithium extraction can be achieved by increasing the upper cutoff voltage. For comparison, the cathode was also cycled without film-forming agents and the voltage profiles are shown in the Supporting Information (Figure S2a). Based on the obtained results, it is confirmed that the parasitic reaction in the unprotected cathode surface is deleterious to the battery performance, and thermally stable film-forming additives protected the cathode surface for achieving stable lithiationdelithiation reactions at extreme-temperature operation (100 °C). Furthermore, performance degradation in an electrolyte containing only LiDFOB may be due to the breaking of CEI layers from continuous high-temperature lithiation-delithiation reactions. This hypothesis was substantiated when the electrode performed stable lithiation-delithiation reactions by attaining synergetic strength from FEC-derived CEI layers. In addition, to evaluate Li metal stability with ionic liquid electrolyte at high temperature, symmetrical Li-Li galvanostatic Li plating/stripping experiment was conducted in pyrrolidinium-based ionic liquid electrolyte without any additives. The electrochemical reaction was carried out at 100 °C. Figure S3 shows the Li plating/stripping reaction at a

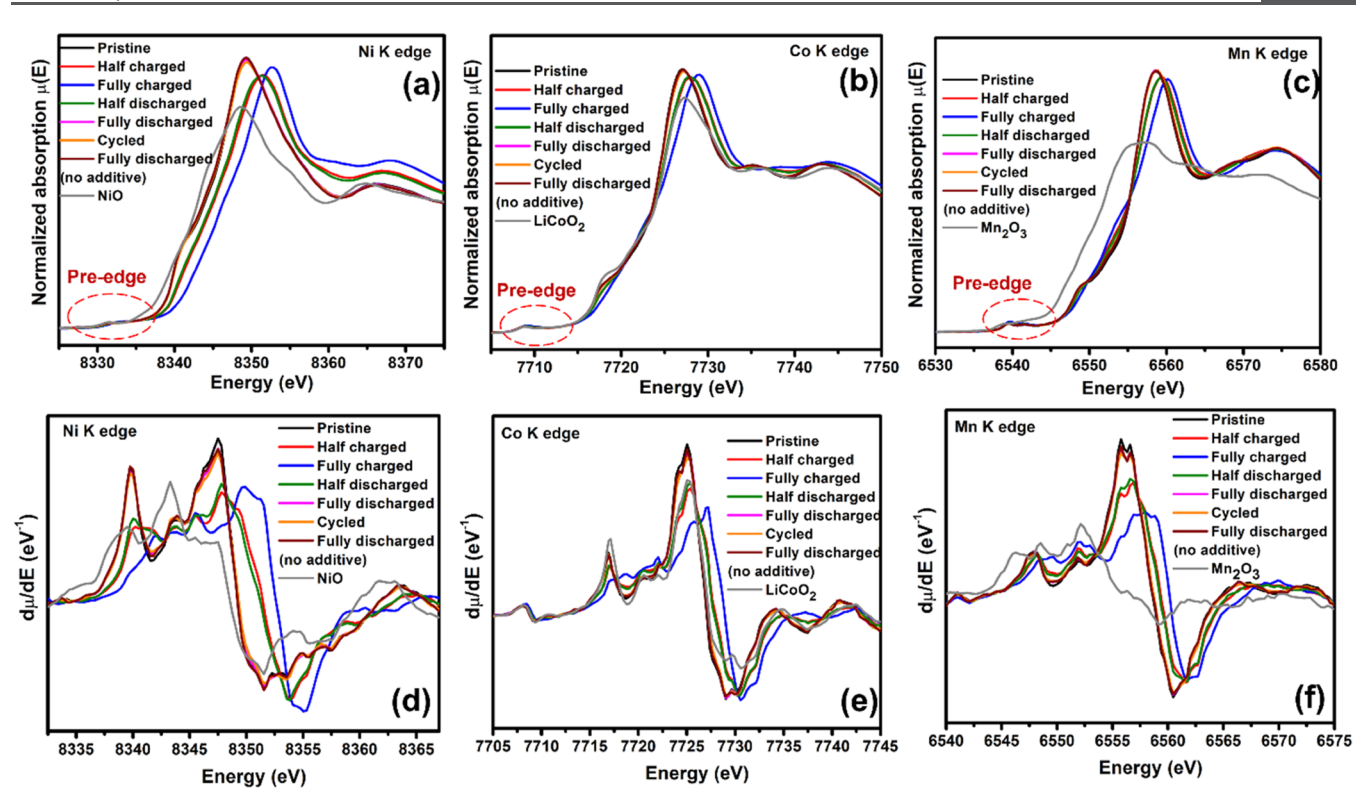


Figure 2. Hard X-ray absorption spectroscopy analysis of the NMC cathode cycled at different conditions. (a) Ni K edge, (b) Co K edge, and (c) Mn K edge XANES spectra. The first derivative of XANES spectra for (d) Ni K edge, (e) Co K edge, and (f) Mn K edge. Pre-edge regions of the transition-metal K edge XANES spectra are shown in Supporting Information Figure S5.

current density of 0.5 mA/cm² and an areal capacity of 0.5 mAh/cm². Interestingly, the results clearly indicate that the overpotential for Li plating/stripping is approximately 25 mV and the overpotential is almost constant for more than 100 h at around 30 mV, resulting in the obtained values being in good agreement with the existing scientific literature evaluated using carbonate electrolytes at room temperature. 41-43 A slight change in polarization during cycling is relatively negligible when compared to the polarization effect observed in the voltage profiles of Figure 1a. This Li plating/stripping behavior at high temperature certainly confirms that the Li metal is reversibly involved in electrochemical reactions without any detrimental parasitic reaction in the presence of the ionic liquid electrolyte. Therefore, it strongly confirms that the origin of huge polarization observed in Figure 1a during high-temperature operation of NMC/Li cell in the ionic liquid electrolyte is mainly due to the parasitic reactions between the ionic liquid and positive electrode rather than negative electrode reactions during initial cycles. In our previously published works, the Li metal anode was successfully used as a reference/counter electrode for understanding high-temperature stable electrode materials in ionic liquid-based electrolytes for Li-ion batteries.^{3,12,18,25,44} In this study, the Li metal anode was used as a reference/counter electrode to investigate the cathode surface of high-temperature lithiation—delithiation reactions. This CEI understanding will be helpful to further develop high-temperature cathode chemistry for specific industrial applications that can be achieved with less reactive and high-temperature stable anodes, especially Li₄Ti₅O₁₂. Hence, in this study, we believe that the combined LiDFOBand FEC-derived CEI layers protect the reactive cathode surface from the electrolyte and unwanted parasitic degradation reactions during high-temperature electrochemical reactions.

Understanding Transition-Metal (TM) Redox Activity: **XANES Study.** After evaluating the electrochemical performance of the NMC cathode at extremely high temperature, identifying possible redox couple contributions toward the obtained specific capacity at 100 °C is of paramount importance. To avoid discrepancy in possible surface-to-bulk charge heterogeneity, initially, we introduced bulk-sensitive hard X-ray synchrotron XAS analysis to identify possible redox reactions at high-temperature operation. The detailed X-ray absorption near-edge structure (XANES) analysis of transitionmetal K edge on a different set of samples including pristine, half-charged, fully charged, half-discharged, completely discharged, cycled state (15 cycles), and fully discharged state without additives is shown in Figure 2. In general, the XANES spectra provide significant information about the electronic structure and local environmental changes in the absorbing atoms of the Li-ion battery electrode material. 45 During high valence states, the core electrons will have strong binding toward the nucleus; therefore, the photoionization process requires more energy to eject the electrons from the core level. 46 Conceivably, when an absorbing atom is at its high oxidation state, the XANES spectra shift to high energy; conversely, a lower oxidation state will shift the XANES spectra toward low energy. In Figure 2, normalized spectra of Ni, Co, and Mn K edge spectra are shown. The XANES spectra can have two major regions: pre-edge region and main absorption edge region. Fundamentally, the pre-edge regions are responsible for the dipole-forbidden transition of 1s-to-3d electronic transition of Ni, Co, and Mn atoms. 47-49 Due to orbital symmetry restriction, the 1s-to-3d transition is limited

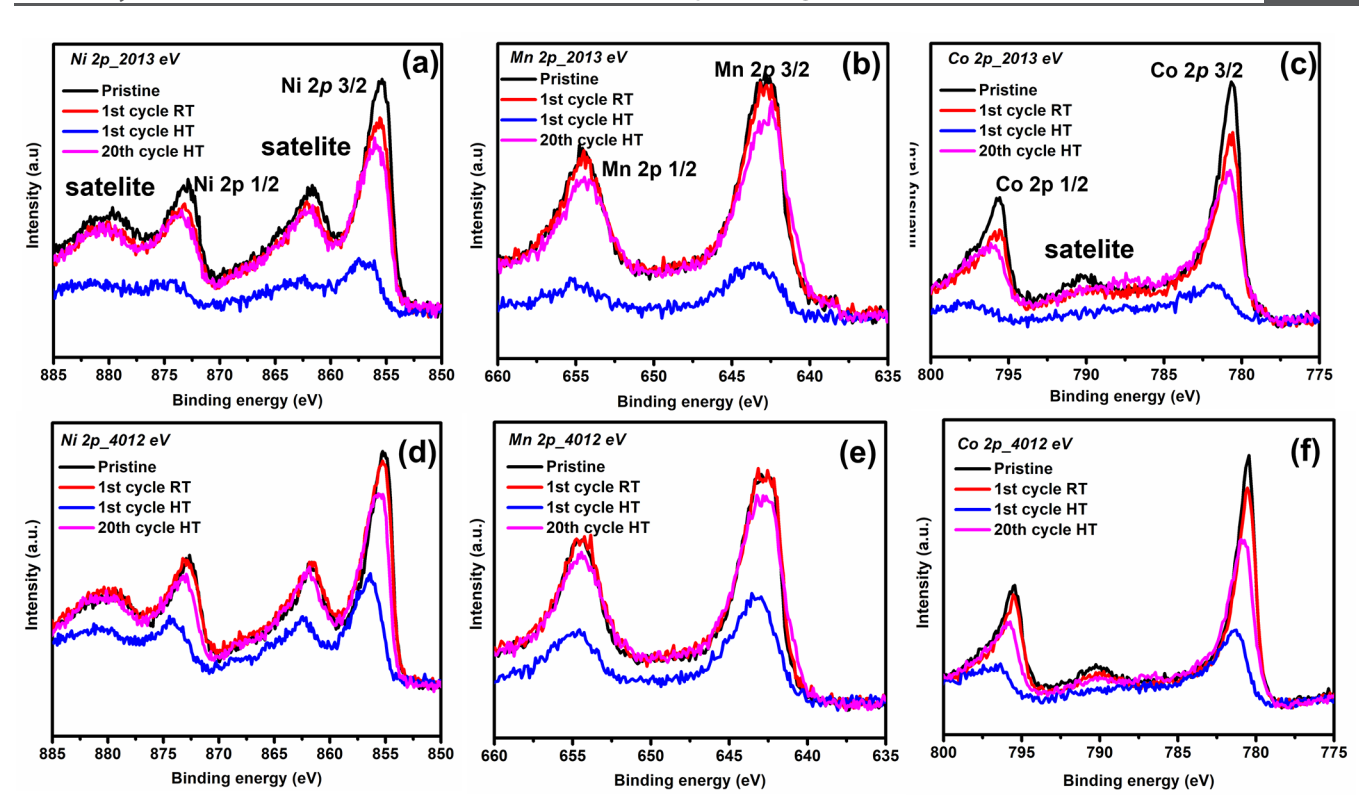


Figure 3. HAXPES spectra of transition-metal 2p for different cycled conditions using different photon energies of 2013 and 4012 eV. (a, d) Ni 2p, (b, e) Mn 2p, and (c, f) Co 2p (HT, high temperature 100 °C, RT, room temperature).

and the pre-edge peaks are observable upon hybridization of d and p orbitals, allowing the electronic dipole transitions from 1s to the hybridized orbital of the p component. 50,51

In general, the pre-edge features provide significant information and can be correlated to coordination number and coordination symmetry. 49 Electronic quadruple transitions will occur in the octahedral symmetry, which is much less intense than the electronic dipole transition in the tetrahedral symmetry. 50 In NMC cathode materials, the metals are in octahedral coordination, resulting in weak pre-edge features in all Ni, Co, and Mn spectra. The shoulder peak observed before the main absorption peak corresponds to the shakedown process involving the dipole-allowed 1s core level to the unoccupied 4p electronic state. Further, the main absorption peak is ascribed to the 1s core level to the unoccupied 4p electronic transition without the shakedown process. 45 As mentioned previously, the edge shift provides information about the average oxidation state of the elements being probed. In Figure 2a, the Ni K edge spectra showed a rigid shift toward high energy during different charged states. The rigid shifts were clearly observed in the derivative plot, as shown in Figure 2d. In the NMC cathode, a major charge contributor is Ni^{2+/4+} ions during charging and discharging in the potential range up to 4.6 V vs Li/Li⁺. 52 During half- and fully charged states, the edge spectra shifted to high energy due to Ni2+ oxidation, indicating that the Ni^{2+/4+} reaction has occurred during hightemperature delithiation. Based on the theoretical and experimental investigation, two-thirds (2/3 or ~66%) of the Li exaction is compensated by Ni^{2+/4+} redox reactions. Similarly, the NMC electrochemical results exhibited ~175 mA/g at 30 mA/g current density, which is similar to the reported capacity value at the same current density in the organic electrolyte.³⁹ According to this obtained capacity, the

extraction ratio is ~62% at 100 °C, indicating that the capacity contribution at extreme temperature is purely from redox centers and not from parasitic reactions as observed in excess capacity in nonpassivated NMC cathodes. Further, during lithiation at 100 °C, the Ni K edge spectra reversibly shifted back to the pristine state, indicating that the cathode electrolyte interphase protects the reactive surface from the electrolyte attack and allows the conventional Ni^{2+/4+} redox reaction reversibly. Compared to Ni K edge, the interpretation of Co and Mn K edge spectra is not straightforward because the edge spectra have no rigid energy shifts during different delithiation levels, and this behavior was reflected in the derivative plots of Co and Mn K edge spectra (Figure 2e,f). However, changes in the pre-edge and edge features are due to changes in the local structural environment such as coordination, symmetry, covalency, and bond length with the ligands. The pre-edge features associated with the transitionmetal K edge XANES are marked in Figure 2, and the corresponding pre-edge regions of transition-metal K edge XANES spectra are shown in Figure S5. Similar to Ni K edge main peak behaviors, the pre-edge feature shifted to high energy during delithiation and exhibited a shift toward lower energy during complete lithiation. In addition, the Mn preedge feature exhibited a characteristic Mn4+ doublet feature and the intensity of this feature is increased during full delithiation and reversibly attained its initial position during full lithiation. This observed pre-edge behavior of the NMC333 cathode cycled under extreme 100 °C is consistent with the layered NMC cathode operated in the organic electrolyte at room temperature. 52 Also, the Co pre-edge feature also exhibited slight intensity changes during different cycling conditions. In NMC333, it is proved that the $Co^{3+/4+}$ is not active and no edge shifts were observed even in the upper

cutoff voltage of approximately 5 V.52 Therefore, we believe that the changes in the edge features are purely from the coordination environment and not from the valence state variation in the bulk of the material (Figure 2b). Further, the Mn K edge spectra are also similar to Co spectra where no rigid energy shifts were observed. In NMC333, it is proved that the Mn ions remain in the tetravalent state during electrochemical delithiation and the changes in the pre-edge features are strongly influenced by the local geometry of the Mn atom. 51,52 Also, the Mn tetravalency was supported with the Mn₂O₃ (Mn^{III}) XANES spectra, which exhibited low edge energy features compared to the NMC cathodes. (Figure 2c). The X-ray absorption results confirm that the redox reactions are primarily from the Ni ions, and the absorption spectra of the sample discharged after one charge-discharge cycle (brown curve) without additives confirmed that the degradation is significantly from surface reactions compared to the bulk of the materials.

Chemistry of Cathode Electrolyte Interphase (CEI): **HAXPES Study.** After analyzing the transition-metal (TM) redox participation through the bulk XAS technique, it is clear that the surface chemistry of the NMC plays a crucial role in the electrochemical performance profile of NMC at high temperatures. To evaluate the surface to near-surface region of the NMC cathode cycled at different conditions, we investigated the NMC cathodes using the energy-tunable hard X-ray photoelectron spectroscopy (HAXPES) technique. Conventionally, XPS is a widely used technique to identify the oxidation state of elements, chemical composition, solid electrolyte interphase, and cathode electrolyte interphase in battery materials. 53,54 However, most of the time, the TM 2p photoelectron spectra are influenced by auger spectra of other elements. For example, in the NMC cathode, the Ni 2p spectra overlap with the F KL_{1,2}L₃ auger line, which leads to misinterpretation of various metal fluoride (MF_r) species in the surface chemistry analysis of battery materials.⁵⁵ Also, the depth dependency of highly sensitive surface layers is analyzed through the destructive milling method, which could modify the local bonding environment at the exposed surfaces. 56-To overcome these experimental challenges, we investigated the NMC cathode using different photon energies ranging from 2000 to 6500 eV.

Transition-Metal Evolution at Different Depth Levels. The TM 2p photoemission spectra collected at 2013 and 4012 eV are shown in Figure 3. In this section, the valence state of the TM and the surface chemistry influence on the photoemission spectral features are studied. From the main peak and satellite peak energy positions, the valence states of the TM could be elucidated.⁵⁹ Fundamentally, the oxidation of TM in these cathode materials changes the metal-ligand hybridization character, which strongly influences the photoemission spectra of the atom being probed. All Ni 2p spectra exhibit similar spectral features except for a sample that is cycled at high temperature for one charge-discharge cycle (Figure 3a,d). This phenomenon is due to the significant surface layer that is formed during the initial CEI formation from the film-forming additives at high temperature, and this surface layer is masking the spectral features of the transition-metal 2p spectral features. 60,61 Interestingly, the NMC cathode cycled at room temperature exhibited no intensity variation even though the electrolyte had similar additives, indicating that the CEI formation is accelerated and formed on the surface of the NMC cathode during initial cycles of high-

temperature operation. Further, this observation was confirmed by the cycled cathode that may be attributed to the stabilized CEI formed on the surface of the NMC cathode at high temperature. The Ni 2p spectra exhibit two main photoemission peaks of $2p_{3/2}$ and $2p_{1/2}$ around 855 and 873 eV, respectively. The well-defined energy separation in TM 2p spectra is due to the spin-orbit coupling into the $2p_{3/2}$ and 2p_{1/2} emissions.^{59,62} Also, strong satellite peaks are located at about 861.7 and 879.8 eV. Fundamentally, the energy difference between the main photoelectron peak and the satellite peaks is strongly correlated with the valence state of the elements. In general, the energy difference of about 6 eV is usually observed for divalent cations and about 10 eV for trivalent and tetravalent cations.⁵⁹ In this work, the energy difference value of 6.6 eV was identified, which implies that the Ni is at 2+ oxidation state Ni^{2+} ($t_{2g}^{}$ $e_{g}^{}$) in pristine. Also, all of the discharged samples exhibit similar energy difference values, which confirms that the majority of the Ni reached their pristine state after involvement in the Ni^{2+/4+} redox couple contribution. Thanks to the energy-tuning ability of the HAXPES technique that eliminated the contribution from the FL₁L₂₃ auger spectral line in Ni 2p spectra. Furthermore, the CEI influence on other transition-metal elements was also investigated at different depth levels. In general, the Mn atom is in NMC as the tetravalent state $(Mn^{4+}/t_{2g}^{3} e_{g}^{0})$ with the ground-state configuration, and the Mn4+ cation is not taking part in the electrochemical reaction operated between 2.8 and 4.3 V vs Li^{+,52} Due to its inactivity, the Mn could be used for understanding the effect of CEI thickness on the spectral features of the TM 2p spectra clearly. The Mn 2p spectra exhibited two definite peaks due to the spin-orbit coupling of photoemission main peaks Mn $2p_{3/2}$ and Mn $2p_{1/2}$, which are located at about 642.7 and 654.5 eV, respectively (Figure 3b,e). The observed main peaks correspond to the Mn⁴⁺ (d³/ t_{2g}^{3} e_{g}^{0}). Similar to Ni 2p spectra, the first cycle at high temperature demonstrated less intensity than other Mn 2p spectra, indicating that the thicker CEI formation significantly affects the spectral features of Mn 2p spectra. Since Mn⁴⁺ is inactive, this photoemission feature is the true nature of the CEI effect on the Mn 2p spectra, which confirms that the initial cycle at high temperature plays a crucial role in CEI formation on the NMC cathode surface. At high photon energies, similar Mn 2p spectral features are observed and the intensity of the first cycle signal improved as the probing depth increases due to the high photon energy. Further, in stoichiometric NMC oxides and LiCoO2, the cobalt cation has a formal valence state of 3+ $(d^6/t_{2g}^6 e_g^6)$ oxidation with low spin electronic configurations. Similar to Mn cation, the Co 3+ is inactive in the potential range used in this study, and it will contribute to the electrochemical lithiation-delithiation reaction at extreme high potentials that will lead to stability issues of the cathodes. Here, the Co 2p peaks split into two main peaks Co $2p_{3/2}$ at about 780.6 eV and Co $2p_{1/2}$ at about 795.6 eV. Further, the satellite peaks near Co 2p_{3/2} were observed at about 790 eV. The energy difference value of approximately 10 eV confirms that most of the Co ions are present in the trivalent oxidation state in the pristine composition and all other cycled states of NMC cathodes. As shown in Figure 3c,f, similar to other TM 2p spectra, the Co 2p spectra are also affected by the thicker CEI formed on the surface of the NMC at high-temperature cycle. Also, the satellite peaks are not clearly observed due to the masking effect of the CEI layer. The main peaks of the cathode after the high-temperature

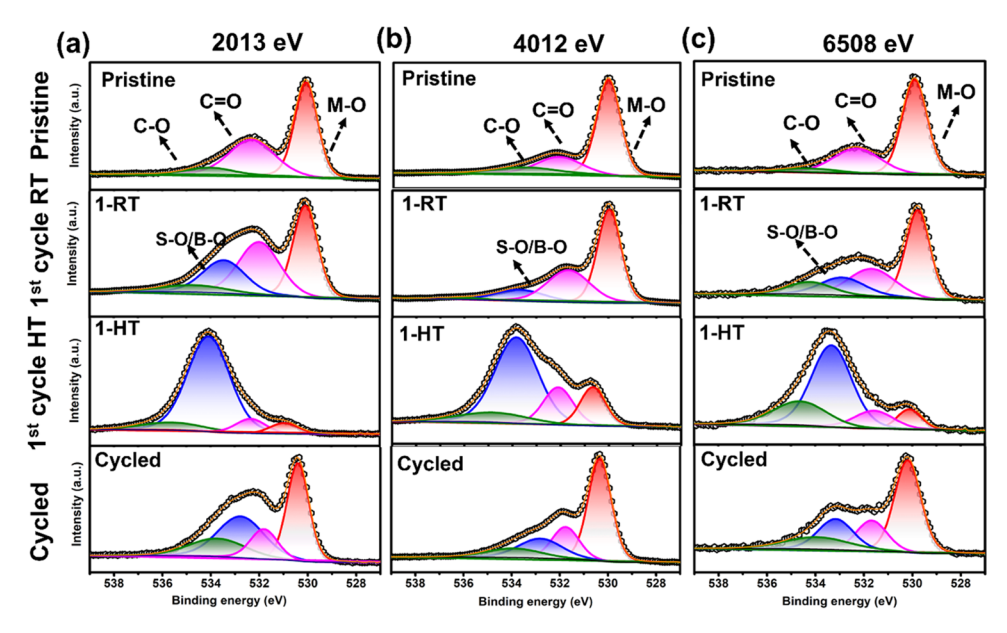


Figure 4. Photoemission spectra of O 1s for different sample conditions and three different photon energies. (a) 2013 eV, (b) 4012 eV, and (c) 6508 eV. (Sample conditions are labeled as pristine, first cycle room temperature: 1-RT, first cycle high temperature: 1-HT, and cycled -20 cycles.).

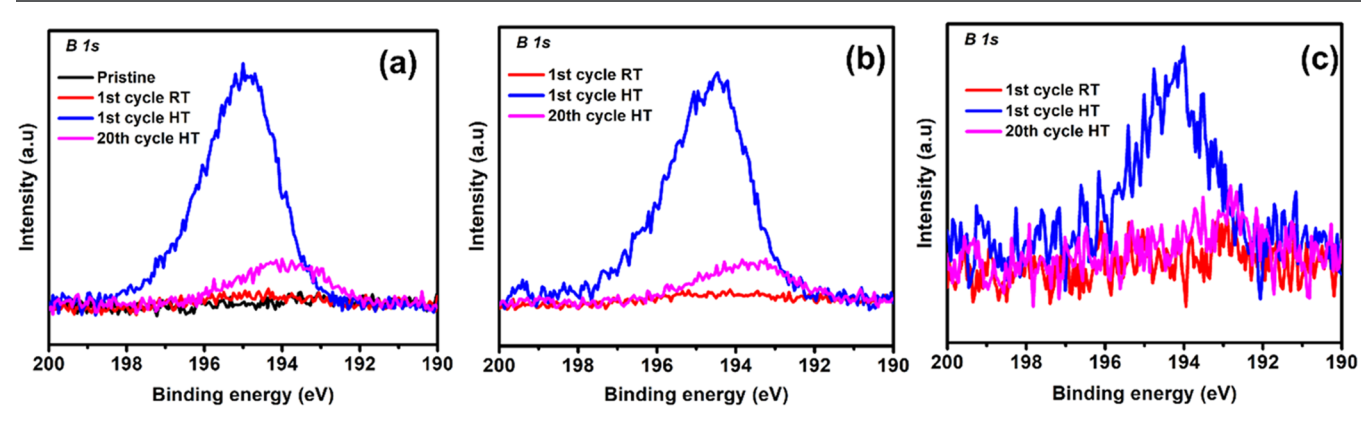


Figure 5. Photoemission spectra of B 1s for different sample conditions and different photon energies. (a) 2013 eV, (b) 4012 eV, and (c) 6508 eV (HT, high temperature 100 °C; RT, room temperature).

initial cycle and satellite peaks of other Co 2p spectra were improved when the photon energy was increased to probe the buried surfaces of the CEI layer. In NMC333, the satellite structure of Co 2p will provide insights into the Co oxidation state; ⁵⁵ the slight changes of satellite structures at low photon energy may be due to the effect of CEI masking on the surface of the cathode particles.

After confirming the CEI presence and TM electronic structure using TM 2p spectra, the depth-dependent CEI chemical composition was investigated by analyzing major CEI constituent elements C 1s, O 1s, F 1s, B 1s, N 1s, and S 1s at different photon energies ranging from 2000 to 6500 eV. Photoemission spectra of O 1s for the pristine sample at three different photon energies are shown in Figure 4a–c. The strong photoemission peak at about 530 eV is assigned to the lattice oxygen (M–O), and the weak photoemission peaks at about 532.2 and 534 eV correspond to the carbon–oxygen functionalities from the conductive carbon and surface functionalities.⁶⁴ When the photon energy is increased from 2013 to 6508 eV, the strong peak at 530 eV does not exhibit any change in the peak structure, indicating that the observed feature is purely from the lattice oxygen (M–O) signal. For

this HAXPES analysis, the pristine first cycle at room temperature, the first cycle at high temperature, and cycled samples are measured using energy-tunable HAXPES techniques. Further, the surface layer species at different photon energies exhibited significant changes in the photoemission signals after different cycling conditions. Based on the peak fitting, we confirmed that the peak around 532 eV is due to the C=O functionality, while the peak at 534 eV is responsible for C-O species. Interestingly, the peak observed between C = O and C-O is possibly due to the S-O and B-O species that are derived from the LiDFOB additive and TFSI⁻ salt anion-derived surface species.^{20,64} In general, the LiDFOB reaction mechanism involves the ring-opening reaction and the formation of borane-based species that interact with the metal oxide surface to form strong B-O functionalities.⁶⁴ Compared to different sample conditions, the initial cycle at 100 °C (sample 1-HT) exhibited strong CEI signal, and the M-O peak is completely suppressed as the observed similar phenomenon in TM 2p analysis (Figures 4ac and 3). This phenomenon confirms that the CEI formation occurs during the initial cycle at high temperature and further the CEI surface chemistry was modified similar to that

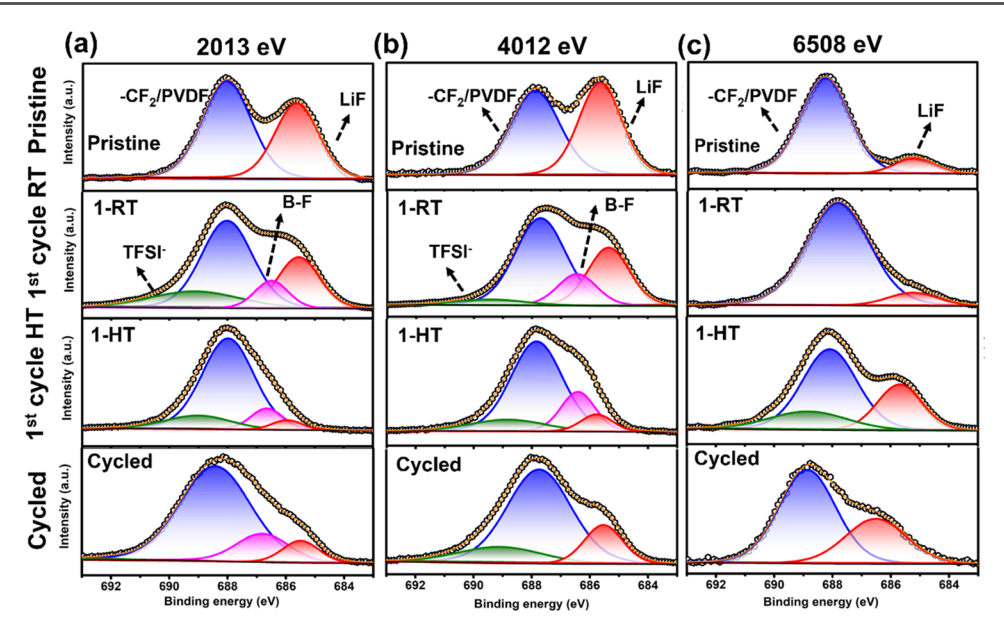


Figure 6. Photoemission spectra of F 1s for different sample conditions and three different photon energies. (a) 2013 eV, (b) 4012 eV, and (c) 6508 eV. (Sample conditions are labeled as pristine, first cycle room temperature: 1-RT, first cycle high temperature: 1-HT, and cycled-20 cycles.).

observed in the electrode cycled at room temperature. This trend is observed in all of the samples at different depth levels. Hence, we hypothesize that the CEI formation is severed from the initial decomposition of surface film-forming additives at high temperature and the initial formation of CEI composition at high temperature is different from the cycled sample.

To understand the effect of boron (B)-based additives in CEI formation at high temperature, the B 1s HAXPES measurements were carried out at different depth levels (Figure 5) in the NMC333 model cathode under different cycling conditions. As expected, the B 1s signal was not observed in the pristine cathode, but the room-temperature cycled electrode exhibits negligible B 1s features compared to high-temperature cycled electrodes. This observation indicates that the additive decomposition and surface layer formation are not accelerated during the initial room-temperature cycling condition. Conversely, the cathode cycled at high temperature during the initial cycle showed intense B 1s features compared to cycled electrodes at high temperature. The significant reduction in the intensity of B 1s features after cycling is mainly attributed to the degradation of the B-rich CEI layer, which protects the reactive cathode surface from an aggressive high-temperature environment. In addition, the B signals were clearly observed at different photon energies, indicating that the B is rich in the CEI layer starting from the bulk of the CEI layer. With the energy tunability of the HAXPES technique, the S 1s spectra could be measured, which cannot be obtained in the conventional XPS technique. The S 1s spectra at different cycled conditions are shown in the Supporting Information (Figure S6). From Figure S6, the S 1s spectra contain two peaks in all of the cycling conditions, a peak about 2472 eV and another peak around 2478 eV corresponding to anionic sulfide species (S2-) and S-O components, respectively. 65,66 The strong signal from S-O around 2478 eV mainly results from the salt anion and additive-derived S-O species in the CEI layer. From the intensity of the S-O peaks, it reveals that the S-O surface layer is from the bulk of the materials rather than surface oxidation-induced S-O species. A clear trend is observed that the intensity of the S 1s

species is well resolved in cycled cathodes compared to a single charge—discharge cycle at room temperature as well as high temperature, implying that the continuous lithiation and delithiation reactions at an extremely high-temperature environment modified the CEI layer and stabilized over extended cycling.

The surface layer was further analyzed with F 1s spectra at different depth levels using multiple photon energies ($h\nu$ = 2013, 4012, and 6508 eV). The F 1s spectra of the samples at different photon energies are shown in Figure 6. As per Figure 6, strong signals around 685 and 688 eV are observed in all of the cycling conditions and photon energies; the pristine composition exhibited CF_x (688 eV) component and LiF (685 eV), which are attributed to the contributions from PVDF binder and LiF, respectively. Further, the cycled samples exhibited CF_r signal due to the contribution from the PVDF binder as well as CEI species with CF_x functionalities.⁶⁷ Furthermore, the pristine composition exhibited LiF component at the surface region and the deeper surface showed less LiF contamination (Figure 6a-c). The LiF contribution in the pristine sample might originate from the reaction between the PVDF binder and the NMC particles during slurry preparation. In the deeper surfaces, the LiF contribution is small, indicating that the reactive surface regions reacted with the PVDF and not the bulk of the NMC particles. Second, the cathode at the RT condition (sample 1-RT) exhibited different fluorinecontaining species at different depth levels (Figure 6a-c). Most surface regions exhibited dominant PVDF and LiF contribution but also additional peaks around 686 and 689 eV are also identified. The observed additional species are due to the additive salt-derived B-F/O-B-F species, and the high binding energy signal is due to the salt anion (TFSI-) contribution from the electrolyte.⁶⁴ Interestingly, the hightemperature cycled sample (sample 1-HT) showed significant change in the peak shapes compared to all other cycled conditions (Figure 6a-c). In this case, the CF_x species contributed significantly and other B-F and LiF indicated smaller contributions, indicating that the CEI formation aggravated at high temperature with more CF_x fluorine-

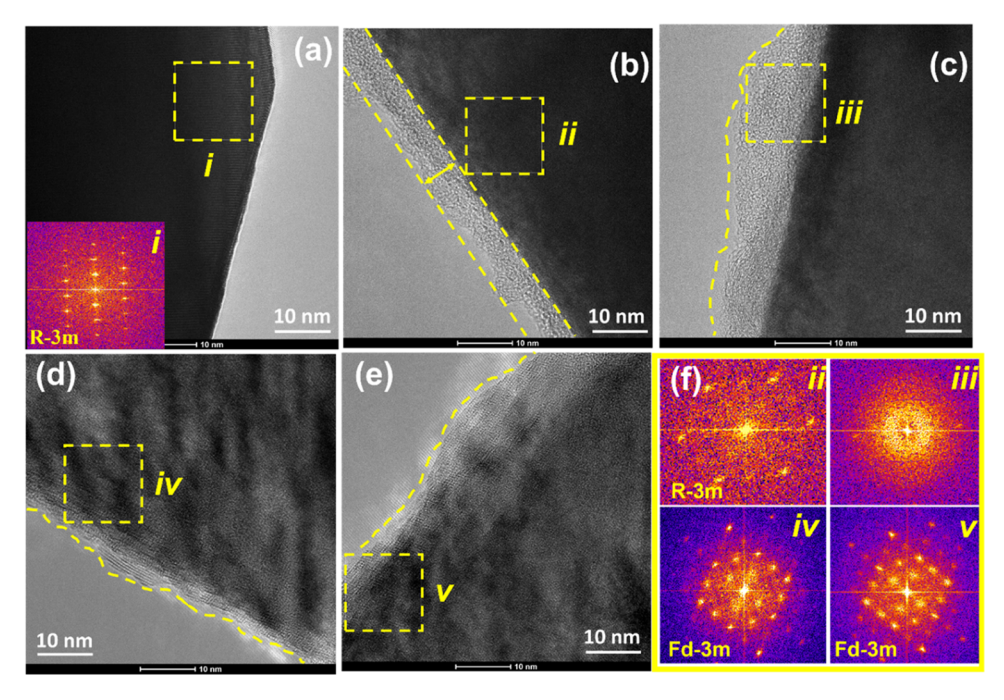


Figure 7. HR-TEM images of the NMC333 cathode cycled at 100 °C with and without cathode electrolyte interphase film-forming additives. (a) Pristine NMC333 cathode powder; (b, c) cycled cathode with film-forming additives; (d, e) cycled cathode without film-forming additives; and (f) FFT patterns of selected regions (ii, iii, iv, v) in the HR-TEM images.

containing species from additive decomposition reactions. The results also indicate that the deep surface of the hightemperature cycled electrode contributed to CFx, TFSI-, and LiF species but no significant B-F species, implying that the B-F species are significantly low at buried surfaces and rich in the surface CEI compositions. This supports the B 1s spectral features observed in Figure 5 where the surface layers consist of dominant B species, but the deeper surfaces indicated only minimal B species. Also, the TFSI- presence was confirmed with N 1s spectra where the observed peak around 400 eV is attributed to the N species from the TFSI- anion and also a slight contribution from N based pyrrolidium cation from the ionic liquid during high-temperature cycling (Figure S8). Finally, the cycled samples are dominated by uniform fluorinecontaining species, but the deeper CEI composition has no B-F or TFSI species, supporting that the DFOB additive anionderived fluorine species predominantly formed on the surface and the TFSI- anion slightly contributed to surface fluorine contributions (sample-cycled). In addition to other soft elements, the main building block element carbon was analyzed with two different photon energies for understanding possible depth-dependent carbonaceous species after different cycling conditions. Based on the C 1s HAXPES studies, the curve fitting was carried out in the C 1s spectral features observed in the different states of cycled cathode materials (Figure S7). The C 1s feature was analyzed with 2013 and 4012 eV photon energies. The features observed at 284.8 and 285 eV are assigned to the conductive carbon species (C-C) from active materials, and the peak at 285.2 eV is responsible for the hydrocarbon functionalities (CH_x).^{68,69} Further, the polyvinylidene difluoride (PVDF) features were observed at around 286 and 291 eV, and the peaks due to C-O and C=O spectral features are observed at about 286.2 and 288 eV, respectively. 20,64,69 According to the different photon energies, the carbon species at pristine materials exhibited negligible differences in spectral features, implying that the pristine

materials do not have any significant compositional variation at different depth levels. Further, the cycled cathode at room temperature showed similar spectral features except the increment in the hydrocarbon functionalities, indicating that the CEI formation was not accelerated at the initial room-temperature reaction. In addition, this similar phenomenon is well observed in the cathode material cycled at high-temperature operation, indicating that the CEI formation is facilitated at high-temperature compared to that at room-temperature operation. Conversely, the cycled electrodes at high temperature showed significant changes in the peak shape and C—O component at 286.2 eV, implying that the cycling of cathode materials at extreme high-temperature operation modifies the cathode electrolyte interphase layer and its composition was varied at different depth levels.

Visualization of Conformal CEI and Failure Mecha**nism: HR-TEM.** After understanding the chemical information of the CEI formed on the surface of the NMC cathode surface, a direct visualization of the CEI that is formed to protect the NMC surface from the electrolyte attack and further structural degradation at extremely high-temperature operating conditions is performed. To visualize the CEI protection ability toward the cathode surface, the HR-TEM investigation was carried out in a different set of cycled NMC samples. As shown in Figure 7, the pristine NMC cathode particle exhibited a clear and well-ordered crystalline layered structure. The surface of the NMC particle is clean and does not show any surface layers or amorphous surface-adsorbed species. Further, the NMC cathode cycled (15 cycles)in 0.8 M pyrrolidinium electrolyte at 100 °C was evaluated. Interestingly, the HR-TEM images of the cycled NMC revealed that the surface region is severely degraded and there is no conformal passivation at the surface to protect the cathode from the reaction between the reactive NMC surface and electrolyte during high-temperature electrochemical reaction (Figure 7d,e). Moreover, the degradation phenomenon not only

occurred at the surface but also occurred through the bulk of the cathode material. On the other hand, the NMC cathode cycled in the ionic liquid electrolyte with film-forming additives showed a uniform CEI layer with a thickness of about 8 nm (Figure 7b,c). The uniform passivation layer is formed on the surface of the cathode due to the decomposition reaction of LiDFOB and FEC film-forming additives at hightemperature operation; this observation was also evidenced by the HAXPES investigation. Further, the fast Fourier transforms (FFTs) of the selected regions in the cathode materials cycled in different conditions are shown in Figure 7f and the inset in Figure 7a. The region (i) in the pristine state exhibited $R\overline{3}m$ layered structure features along the [110] orientation. In addition, after cycling with high-temperature-compatible surface passivation, the FFT regions in the cathode surface retained $R\overline{3}m$ structural features (ii), and the amorphous nature of CEI was confirmed by the FFT region (iii) where the data showed only an amorphous halo rather than any reflections. When comparing this with the degraded surface of cathode materials, the structural deviations were clearly identified as the FFT regions near the surface demonstrating a spinel structural feature $(Fd\overline{3}m)$ along the [110] orientation (iv, v). From this observation, it is confirmed that the structural degradation during high-temperature cycling transformed the structural features from layered to spinel on the surface of the particle. This observed phenomenon could also be correlated with the poor electrochemical performance of the cathodes without surface passivation. To date, the layer-tospinal structural transformation is considered to be a daunting issue in various layered cathode materials at extreme cycling conditions. 70,71 Based on the above discussion, it is clear that the thermally stable cathode electrolyte interphase layer on the surface protects the NMC surface from the direct contact between the electrolyte and further degradation of cathode particles during high-temperature lithiation-delithiation reactions. In general, the Ni redox-based NMC cathodes suffer from various parasitic reaction-induced degradation mechanisms even at room temperature. 40,72 In this work, the NMC cathode was cycled in a practical potential region of 2.8-4.3 V but operated in an extreme high-temperature operation of 100 °C. The observed degradation mechanisms in Ni redox cathodes are not unique and they are highly interdependent. It is difficult to rationalize a single factor for the degradation mechanism of NMC with the currently available knowledge. Among various degradation mechanisms, parasitic reactions due to surface impurity, TM dissolution, redox couple evolution, parasitic reaction of Ni4+ with the electrolyte, and CO₂ generation were identified as serious issues in Ni redox cathodes. 40 Based on the experimental observation, we believe that a failure mechanism of the NMC cathode at high temperature has a strong correlation with the parasitic reactions at high temperature. As mentioned, Ni redox is a this understanding, we hypothesize that the highly reactive Ni redox with fluorine-rich ionic liquids may react together at extreme high temperature. Even though ionic liquids are highly stable in the operated potential region, the high-temperature delithiation may trigger parasitic reactions between the highly delithiated NMC with the electrolyte. In addition, high valent

 ${
m Co}^{3+}$ and ${
m Mn}^{4+}$ are present in the NMC cathode and their reactivity of redox couple evolutions at extreme temperature is questionable. Interestingly, in this work, the reversible lithiation/delithiation reaction of NMC at 100 ${
m ^{\circ}C}$ is achieved by identifying appropriate additives, which produce thermally stable conformal CEI layers on the NMC surface to protect the cathode from parasitic reaction-induced degradations.

CEI Formation Mechanism. In this work, the hightemperature performance of the NMC333 cathode was investigated with the stabilized electrode/electrolyte interface layer. The fundamental mechanism is reducing the direct contact between the reactive NMC cathode surface and electrolyte at the extreme high-temperature electrochemical reaction using the cathode electrolyte interphase film formed from the decomposition products of functional additives. First, the LiDFOB and FEC additives were introduced into the ionic liquid mixture and the decomposition products from the additives formed a stable surface layer on the NMC cathode surface during high-temperature electrochemical reactions. Conventionally, the LiDFOB is identified as a surface filmforming additive by combining the merits of lithium bis-(oxalato)borate (LiBOB) and lithium tetrafluoro borate LiBF₄. ⁷³ Due to the lower anodic stability (<4.4 V vs Li/Li +) of LiDFOB, the lithium conducting salt is used as a CEI film-forming additive in high-voltage cathode materials because the salt tends to form a stable surface film on the cathode surface (CEI) that will reduce the direct contact between the reactive cathode surface and electrolyte by surface passivation. ^{29,33} In addition, the introduction of FEC in the electrolyte improved the electrolyte performance of NMC at high temperature. In general, the FEC is known as an anode passivating agent; however, the FEC addition in the carbonate electrolyte is also considered for cathodes and attracted interest due to its film-forming ability at the cathode side during electrochemical reactions. 35-37,61,74,75 Similarly, this slight performance increment after FEC addition may also be due to the effect of its passivation on the lithium reference electrode and NMC positive electrode at high-temperature lithiation-delithiation reactions. However, the decomposition products of electrolyte additives in the ionic liquid environment indicate the formation of CEI products mainly with carbon-, oxygen-, boron-, and fluorine-containing surface species. This observation was confirmed by depth analysis of the NMC cathode at different cycling conditions. Therefore, the synergetic effect of film-forming additives in extreme high temperate indicates that the reactive NMC surface could be tailored with the thermally stable electrode-electrolyte interface for exploring extreme-temperature Li-ion batteries from transforming ambient-temperature technologies.

CONCLUSIONS

High-temperature operation of NMC is a long-standing issue where the cathode material becomes unstable and produces gases such as CO, CO₂, and O₂ as a result of high-temperature degradation. The unwanted gaseous products then react with the electrolyte species at high temperature and accelerate the parasitic reaction-induced degradation in both electrolyte components and electrode materials. To address this fundamental issue, we proposed a thermally stable CEI formation that prevents the highly oxidized cation from contact with the electrolyte, thereby mitigating parasitic reactions at elevated temperatures. To prove this concept, we investigated the NMC333 at an extreme temperature of

100 °C and found that the NMC333 is degrading much faster that leads to not even withstanding 5 cycles at hightemperature operation. Interestingly, the ionic liquid consists of CEI-forming additives that stabilized the NMC surface by forming a stable highly Li-ion conducting passivation layer and allowing reversible lithiation-delithiation reactions at a hightemperature operation of 100 °C. With this technological achievement, the surface and bulk properties of NMC cathodes were analyzed using advanced spectroscopy and microscopy probes. From the hard X-ray XANES study, the Ni K edge spectra showed a rigid shift toward high energy during different charged states. During half- and fully charged states, the edge spectra shifted to high energy due to Ni²⁺ oxidation, indicating that the Ni^{2+/4+} reaction has occurred during high-temperature delithiation. The NMC electrochemical results exhibited 175 mA/g at 30 mA/g current density, which is similar to the reported capacity value at the same current density in organic electrolytes. According to this obtained capacity, the extraction ratio is 62% at 100 °C, indicating that the capacity contribution at extreme temperature is purely from Ni redox center and not from parasitic reactions as observed excess capacity in nonpassivated NMC cathodes. Further, the HAXPES studies revealed that the conformal CEI formation on a cathode surface is accelerated during initial cycles at hightemperature compared to those at room-temperature cycling. The depth-dependent boron- and fluorine-based CEI compositions were identified, and their conformal passivation ability on the NMC cathode surface was visualized with HR-TEM investigation, unveiling that the CEI protects the reactive surface from the electrolyte attack and allows the reversible lithiation and delithiation reactions at an extremely high temperature of 100 °C. With these fundamental results, we believe that this present work unravels the challenges associated with high-temperature battery materials and will pave the way for transforming ambient-temperature technology into extreme-temperature applications.

ASSOCIATED CONTENT

Supporting Information

The Supporting Information is available free of charge at https://pubs.acs.org/doi/10.1021/acs.chemmater.2c00435.

X-ray powder diffraction of the NMC cathode, charge—discharge profiles of the NMC333 cathode without additives, comparison of capacity evolution and Coulombic efficiency plots, symmetrical cell Li—Li galvanostatic Li plating/stripping results, photographs of prepared electrolytes, pre-edge regions of transitionmetal K edge spectra, S 1s HAXPES spectra at 6508 eV, C 1s HAXPES spectra at 2013 and 4012 eV, and N 1s HAXPES spectra of the NMC333 cathode (PDF)

AUTHOR INFORMATION

Corresponding Author

Leela Mohana Reddy Arava — Department of Mechanical Engineering, Wayne State University, Detroit, Michigan 48202, United States; orcid.org/0000-0001-6685-6061; Email: leela.arava@wayne.edu

Authors

Sudhan Nagarajan — Department of Mechanical Engineering, Wayne State University, Detroit, Michigan 48202, United States; Occid.org/0000-0002-3524-5062

Conan Weiland – Material Measurement Laboratory, National Institute of Standards and Technology, Gaithersburg, Maryland 20899, United States

Sooyeon Hwang — Center for Functional Nanomaterials, Brookhaven National Laboratory, Upton, New York 11973, United States; orcid.org/0000-0001-5606-6728

Mahalingam Balasubramanian — X-ray Science Division, Advanced Photon Source, Argonne National Laboratory, Lemont, Illinois 60439, United States; Present Address: Electrification and Energy Infrastructure Division, Oak Ridge National Laboratory, Oak Ridge, Tennessee 37830, United States; ⊚ orcid.org/0000-0002-3988-3125

Complete contact information is available at: https://pubs.acs.org/10.1021/acs.chemmater.2c00435

Notes

Commercial equipment, instruments, and materials are identified in this paper to fully specify the experimental procedure and do not represent an endorsement by the National Institute of Standards and Technology. The authors declare no competing financial interest.

ACKNOWLEDGMENTS

This material was based upon work supported by the National Science Foundation under grant number 1751472. The authors also acknowledge funding support from the Advanced Energy Consortium (AEC) (BEG14-02). http://www.beg. utexas.edu/aec/partners companies include BHP, ExxonMobil, U.S. Department of Energy, Repsol, Sandia National Labs, and Total. This research used resources of the National Synchrotron Light Source II (NSLS-II), a U.S. Department of Energy (DOE) Office of Science User Facility operated for the DOE Office of Science by Brookhaven National Laboratory under Contract DE-SC0012704. The HAXPES measurements were performed at the National Institute of Standards and Technology (NIST) beamline SST-2 in the NSLS-II. This research also used resources of the Center for Functional Nanomaterials, which is a U.S. DOE Office of Science Facility, at Brookhaven National Laboratory under Contract No. DE-SC0012704. This research used resources of the Advanced Photon Source (APS), an Office of Science User Facility operated for the U.S. Department of Energy (DOE) Office of Science by Argonne National Laboratory under Contract No. DE-AC02-06CH11357. The authors acknowledge the Lumigen Instrument Centre at Wayne State University for the use of XRD (NSF: MRI 1427926) facility.

REFERENCES

- (1) Tarascon, J. M.; Armand, M. Issues and Challenges Facing Rechargeable Lithium Batteries. *Nature* **2001**, *414*, 359–367.
- (2) Goodenough, J. B.; Park, K.-S. The Li-Ion Rechargeable Battery: A Perspective. J. Am. Chem. Soc. 2013, 135, 1167–1176.
- (3) Lin, X.; Salari, M.; Arava, L. M. R.; Ajayan, P. M.; Grinstaff, M. W. High Temperature Electrical Energy storage: Advances, Challenges, and Frontiers. *Chem. Soc. Rev.* **2016**, *45*, 5848–5887.
- (4) Yabuuchi, N.; Ohzuku, T. Electrochemical Behaviors of LiCo1/3Ni1/3Mn1/3O2 in Lithium Batteries at Elevated Temperatures. *J. Power Sources* **2005**, *146*, 636–639.
- (5) Genieser, R.; Ferrari, S.; Loveridge, M.; Beattie, S. D.; Beanland, R.; Amari, H.; West, G.; Bhagat, R. Lithium ion Batteries (NMC/graphite) cycling at 80 °C: Different Electrolytes and Related Degradation Mechanism. *J. Power Sources* **2018**, *373*, 172–183.

- (6) Wright, D. R.; Garcia-Araez, N.; Owen, J. R. Review on High Temperature Secondary Li-ion Batteries. *Energy Procedia* **2018**, *151*, 174–181.
- (7) Bodenes, L.; Naturel, R.; Martinez, H.; Dedryvère, R.; Menetrier, M.; Croguennec, L.; Pérès, J.-P.; Tessier, C.; Fischer, F. Lithium Secondary Batteries Working at Very High Temperature: Capacity Fade and Understanding of Aging Mechanisms. *J. Power Sources* **2013**, 236, 265–275.
- (8) Fan, X.; Chen, L.; Borodin, O.; Ji, X.; Chen, J.; Hou, S.; Deng, T.; Zheng, J.; Yang, C.; Liou, S.-C.; Amine, K.; Xu, K.; Wang, C. Non-Flammable Electrolyte Enables Li-Metal Batteries with Aggressive Cathode Chemistries. *Nat. Nanotechnol.* **2018**, *13*, 715–722.
- (9) Xu, K. Electrolytes and Interphases in Li-Ion Batteries and Beyond. Chem. Rev. 2014, 114, 11503-11618.
- (10) Zhang, Z.; Hu, L.; Wu, H.; Weng, W.; Koh, M.; Redfern, P. C.; Curtiss, L. A.; Amine, K. Fluorinated Electrolytes for 5 V Lithium-ion Battery Chemistry. *Energy Environ. Sci.* **2013**, *6*, 1806–1810.
- (11) Fan, X.; Ji, X.; Chen, L.; Chen, J.; Deng, T.; Han, F.; Yue, J.; Piao, N.; Wang, R.; Zhou, X.; Xiao, X.; Chen, L.; Wang, C. All-Temperature Batteries Enabled by Fluorinated Electrolytes with Non-Polar Solvents. *Nat. Energy* **2019**, *4*, 882–890.
- (12) Ababtain, K.; Babu, G.; Lin, X.; Rodrigues, M.-T. F.; Gullapalli, H.; Ajayan, P. M.; Grinstaff, M. W.; Arava, L. M. R. Ionic Liquid—Organic Carbonate Electrolyte Blends To Stabilize Silicon Electrodes for Extending Lithium Ion Battery Operability to 100 °C. ACS Appl. Mater. Interfaces 2016, 8, 15242–15249.
- (13) Chagnes, A.; Diaw, M.; Carré, B.; Willmann, P.; Lemordant, D. Imidazolium-Organic Solvent Mixtures as Electrolytes for Lithium Batteries. *J. Power Sources* **2005**, *145*, 82–88.
- (14) Elia, G. A.; Ulissi, U.; Jeong, S.; Passerini, S.; Hassoun, J. Exceptional Long-Life Performance of Lithium-ion Batteries using Ionic Liquid-Based Electrolytes. *Energy Environ. Sci.* **2016**, *9*, 3210–3220.
- (15) Lahiri, A.; Schubert, T. J. S.; Iliev, B.; Endres, F. LiTFSI in 1-butyl-1-methylpyrrolidinium bis(fluorosulfonyl)amide: A Possible Electrolyte for Ionic Liquid Based Lithium Ion Batteries. *Phys. Chem. Chem. Phys.* **2015**, *17*, 11161–11164.
- (16) Watanabe, M.; Thomas, M. L.; Zhang, S.; Ueno, K.; Yasuda, T.; Dokko, K. Application of Ionic Liquids to Energy Storage and Conversion Materials and Devices. *Chem. Rev.* **2017**, *117*, 7190–7239.
- (17) Sun, H.; Zhu, G.; Zhu, Y.; Lin, M.-C.; Chen, H.; Li, Y.-Y.; Hung, W. H.; Zhou, B.; Wang, X.; Bai, Y.; Gu, M.; Huang, C.-L.; Tai, H.-C.; Xu, X.; Angell, M.; Shyue, J.-J.; Dai, H. High-Safety and High-Energy-Density Lithium Metal Batteries in a Novel Ionic-Liquid Electrolyte. *Adv. Mater.* **2020**, 32, No. 2001741.
- (18) Rodrigues, M.-T. F.; Kalaga, K.; Gullapalli, H.; Babu, G.; Reddy, A. L. M.; Ajayan, P. M. Hexagonal Boron Nitride-Based Electrolyte Composite for Li-Ion Battery Operation from Room Temperature to 150 °C. Adv. Energy Mater. 2016, 6, No. 1600218.
- (19) Cao, X.; He, X.; Wang, J.; Liu, H.; Röser, S.; Rad, B. R.; Evertz, M.; Streipert, B.; Li, J.; Wagner, R.; Winter, M.; Cekic-Laskovic, I. High Voltage LiNi0.5Mn1.5O4/Li4Ti5O12 Lithium Ion Cells at Elevated Temperatures: Carbonate- versus Ionic Liquid-Based Electrolytes. ACS Appl. Mater. Interfaces 2016, 8, 25971–25978.
- (20) Wu, F.; Kim, G.-T.; Diemant, T.; Kuenzel, M.; Schür, A. R.; Gao, X.; Qin, B.; Alwast, D.; Jusys, Z.; Behm, R. J.; Geiger, D.; Kaiser, U.; Passerini, S. Reducing Capacity and Voltage Decay of Co-Free Li1.2Ni0.2Mn0.6O2 as Positive Electrode Material for Lithium Batteries Employing an Ionic Liquid-Based Electrolyte. *Adv. Energy Mater.* **2020**, *10*, No. 2001830.
- (21) Huang, Q.; Lee, Y.-Y.; Gurkan, B. Pyrrolidinium Ionic Liquid Electrolyte with Bis(trifluoromethylsulfonyl)imide and Bis(fluorosulfonyl)imide Anions: Lithium Solvation and Mobility, and Performance in Lithium Metal—Lithium Iron Phosphate Batteries. *Ind. Eng. Chem. Res.* **2019**, *58*, 22587—22597.
- (22) Zheng, Q.; Yamada, Y.; Shang, R.; Ko, S.; Lee, Y.-Y.; Kim, K.; Nakamura, E.; Yamada, A. A Cyclic Phosphate-Based Battery

- Electrolyte for High Voltage and Safe Operation. *Nat. Energy* **2020**, *5*, 291–298.
- (23) Deng, T.; Fan, X.; Cao, L.; Chen, J.; Hou, S.; Ji, X.; Chen, L.; Li, S.; Zhou, X.; Hu, E.; Su, D.; Yang, X.-Q.; Wang, C. Designing In-Situ-Formed Interphases Enables Highly Reversible Cobalt-Free LiNiO2 Cathode for Li-ion and Li-metal Batteries. *Joule* **2019**, *3*, 2550–2564.
- (24) Shkrob, I. A.; Han, B.; Sahore, R.; Tornheim, A. P.; Zhang, L.; Abraham, D. P.; Dogan, F.; Zhang, Z.; Liao, C. Facile in Situ Syntheses of Cathode Protective Electrolyte Additives for High Energy Density Li-Ion Cells. *Chem. Mater.* **2019**, *31*, 2459–2468.
- (25) Rodrigues, M.-T. F.; Babu, G.; Gullapalli, H.; Kalaga, K.; Sayed, F. N.; Kato, K.; Joyner, J.; Ajayan, P. M. A Materials Perspective on Li-ion Batteries at Extreme Temperatures. *Nat. Energy* **2017**, *2*, No. 17108.
- (26) Yang, J.; Liu, Q.; Pupek, K. Z.; Dzwiniel, T. L.; Dietz Rago, N. L.; Cao, J.; Dandu, N.; Curtiss, L.; Liu, K.; Liao, C.; Zhang, Z. Molecular Engineering to Enable High-Voltage Lithium-Ion Battery: From Propylene Carbonate to Trifluoropropylene Carbonate. *ACS Energy Lett.* **2021**, *6*, 371–378.
- (27) Kim, J.-M.; Zhang, X.; Zhang, J.-G.; Manthiram, A.; Meng, Y. S.; Xu, W. A Review on the Stability and Surface Modification of Layered Transition-Metal Oxide Cathodes. *Mater. Today* **2021**, *46*, 155–182.
- (28) Zheng, J.; Engelhard, M. H.; Mei, D.; Jiao, S.; Polzin, B. J.; Zhang, J.-G.; Xu, W. Electrolyte Additive Enabled Fast Charging and Stable Cycling Lithium Metal Batteries. *Nat. Energy* **2017**, *2*, No. 17012.
- (29) Gao, H.; Maglia, F.; Lamp, P.; Amine, K.; Chen, Z. Mechanistic Study of Electrolyte Additives to Stabilize High-Voltage Cathode—Electrolyte Interface in Lithium-Ion Batteries. *ACS Appl. Mater. Interfaces* **2017**, *9*, 44542—44549.
- (30) Kim, K.; Ma, H.; Park, S.; Choi, N.-S. Electrolyte-Additive-Driven Interfacial Engineering for High-Capacity Electrodes in Lithium-Ion Batteries: Promise and Challenges. *ACS Energy Lett.* **2020**, *5*, 1537–1553.
- (31) Ravel, B.; Newville, M. ATHENA, ARTEMIS, HEPHAESTUS: Data Analysis for X-ray Absorption Spectroscopy using IFEFFIT. *J. Synchrotron Radiat.* **2005**, *12*, 537–541.
- (32) Kraft, S.; Stümpel, J.; Becker, P.; Kuetgens, U. High Resolution X-ray Absorption Spectroscopy with Absolute Energy Calibration for the Determination of Absorption Edge Energies. *Rev. Sci. Instrum.* **1996**, *67*, *681*–*687*.
- (33) Amine, K.; Chen, Z.; Zhang, Z.; Liu, J.; Lu, W.; Qin, Y.; Lu, J.; Curtis, L.; Sun, Y.-K. Mechanism of Capacity Fade of MCMB/Li1.1[Ni1/3Mn1/3Co1/3]0.9O2cell at Elevated Temperature and Additives to Improve its Cycle Life. *J. Mater. Chem.* **2011**, *21*, 17754–17759
- (34) Xu, G.; Liu, Z.; Zhang, C.; Cui, G.; Chen, L. Strategies for Improving the Cyclability and Thermo-Stability of LiMn2O4-based Batteries at Elevated Temperatures. *J. Mater. Chem. A* **2015**, *3*, 4092–4123.
- (35) Etacheri, V.; Haik, O.; Goffer, Y.; Roberts, G. A.; Stefan, I. C.; Fasching, R.; Aurbach, D. Effect of Fluoroethylene Carbonate (FEC) on the Performance and Surface Chemistry of Si-Nanowire Li-Ion Battery Anodes. *Langmuir* **2012**, *28*, 965–976.
- (36) Hu, L.; Zhang, Z.; Amine, K. Fluorinated Electrolytes for Li-ion battery: An FEC-based Electrolyte for High Voltage LiNi0.5M-n1.5O4/Graphite Couple. *Electrochem. Commun.* **2013**, 35, 76–79.
- (37) Shin, H.; Park, J.; Sastry, A. M.; Lu, W. Effects of Fluoroethylene Carbonate (FEC) on Anode and Cathode Interfaces at Elevated Temperatures. *J. Electrochem. Soc.* **2015**, *162*, A1683—A1692.
- (38) Qian, Y.; Niehoff, P.; Börner, M.; Grützke, M.; Mönnighoff, X.; Behrends, P.; Nowak, S.; Winter, M.; Schappacher, F. M. Influence of Electrolyte Additives on the Cathode Electrolyte Interphase (CEI) Formation on LiNi1/3Mn1/3Co1/3O2 in Half Cells with Li Metal Counter Electrode. *J. Power Sources* **2016**, 329, 31–40.

- (39) Kasnatscheew, J.; Röser, S.; Börner, M.; Winter, M. Do Increased Ni Contents in LiNixMnyCozO2 (NMC) Electrodes Decrease Structural and Thermal Stability of Li Ion Batteries? A Thorough Look by Consideration of the Li+ Extraction Ratio. ACS Appl. Energy Mater. 2019, 2, 7733–7737.
- (40) Li, T.; Yuan, X.-Z.; Zhang, L.; Song, D.; Shi, K.; Bock, C. Degradation Mechanisms and Mitigation Strategies of Nickel-Rich NMC-Based Lithium-Ion Batteries. *Electrochem. Energy Rev.* **2020**, 3, 43–80.
- (41) Liang, Z.; Lin, D.; Zhao, J.; Lu, Z.; Liu, Y.; Liu, C.; Lu, Y.; Wang, H.; Yan, K.; Tao, X.; Cui, Y. Composite Lithium Metal Anode by Melt Infusion of Lithium into a 3D Conducting Scaffold with Lithiophilic Coating. *Proc. Natl. Acad. Sci. U.S.A.* **2016**, *113*, 2862–2867.
- (42) Gao, Y.; Zhao, Y.; Li, Y. C.; Huang, Q.; Mallouk, T. E.; Wang, D. Interfacial Chemistry Regulation via a Skin-Grafting Strategy Enables High-Performance Lithium-Metal Batteries. *J. Am. Chem. Soc.* **2017**, *139*, 15288–15291.
- (43) Rajendran, S.; Tang, Z.; George, A.; Cannon, A.; Neumann, C.; Sawas, A.; Ryan, E.; Turchanin, A.; Arava, L. M. R. Inhibition of Lithium Dendrite Formation in Lithium Metal Batteries via Regulated Cation Transport through Ultrathin Sub-Nanometer Porous Carbon Nanomembranes. *Adv. Energy Mater.* **2021**, *11*, No. 2100666.
- (44) Kalaga, K.; Rodrigues, M.-T. F.; Gullapalli, H.; Babu, G.; Arava, L. M. R.; Ajayan, P. M. Quasi-Solid Electrolytes for High Temperature Lithium Ion Batteries. *ACS Appl. Mater. Interfaces* **2015**, *7*, 25777–25783.
- (45) Nam, K.-W.; Bak, S.-M.; Hu, E.; Yu, X.; Zhou, Y.; Wang, X.; Wu, L.; Zhu, Y.; Chung, K.-Y.; Yang, X.-Q. Combining In Situ Synchrotron X-Ray Diffraction and Absorption Techniques with Transmission Electron Microscopy to Study the Origin of Thermal Instability in Overcharged Cathode Materials for Lithium-Ion Batteries. Adv. Funct. Mater. 2013, 23, 1047–1063.
- (46) Alvarado, J.; Wei, C.; Nordlund, D.; Kroll, T.; Sokaras, D.; Tian, Y.; Liu, Y.; Doeff, M. M. Thermal Stress-Induced Charge and Structure Heterogeneity in Emerging Cathode Materials. *Mater. Today* **2020**, *35*, 87–98.
- (47) van Oversteeg, C. H. M.; Doan, H. Q.; de Groot, F. M. F.; Cuk, T. In situ X-ray Absorption Spectroscopy of Transition Metal Based Water Oxidation Catalysts. *Chem. Soc. Rev.* **2017**, *46*, 102–125.
- (48) de Groot, F.; Vankó, G.; Glatzel, P. The 1s X-ray Absorption Pre-edge Structures in Transition Metal Oxides. *J. Phys.: Condens. Matter* 2009, 21, No. 104207.
- (49) Tian, C.; Xu, Y.; Kan, W. H.; Sokaras, D.; Nordlund, D.; Shen, H.; Chen, K.; Liu, Y.; Doeff, M. Distinct Surface and Bulk Thermal Behaviors of LiNi0.6Mn0.2Co0.2O2 Cathode Materials as a Function of State of Charge. ACS Appl. Mater. Interfaces 2020, 12, 11643—11656
- (50) Yamamoto, T. Assignment of Pre-edge Peaks in K-edge X-ray Absorption Spectra of 3d Transition Metal Compounds: Electric Dipole Or Quadrupole? *X-Ray Spectrom.* **2008**, *37*, 572–584.
- (51) Deb, A.; Bergmann, U.; Cramer, S. P.; Cairns, E. J. In situ X-ray Absorption Spectroscopic Study of the Li[Ni1/3Co1/3Mn1/3]O2 Cathode Material. *J. Appl. Phys.* **2005**, *97*, No. 113523.
- (52) Yoon, W.-S.; Balasubramanian, M.; Chung, K. Y.; Yang, X.-Q.; McBreen, J.; Grey, C. P.; Fischer, D. A. Investigation of the Charge Compensation Mechanism on the Electrochemically Li-Ion Deintercalated Li1-xCo1/3Ni1/3Mn1/3O2 Electrode System by Combination of Soft and Hard X-ray Absorption Spectroscopy. *J. Am. Chem. Soc.* 2005, 127, 17479–17487.
- (53) Philippe, B.; Hahlin, M.; Edström, K.; Gustafsson, T.; Siegbahn, H.; Rensmo, H. Photoelectron Spectroscopy for Lithium Battery Interface Studies. *J. Electrochem. Soc.* **2016**, *163*, A178–A191.
- (54) Edström, K.; Gustafsson, T.; Thomas, J. O. The Cathode–Electrolyte Interface in the Li-ion Battery. *Electrochim. Acta* **2004**, *50*, 397–403
- (55) Bondarchuk, O.; LaGrow, A. P.; Kvasha, A.; Thieu, T.; Ayerbe, E.; Urdampilleta, I. On the X-ray Photoelectron Spectroscopy

- Analysis of LiNixMnyCozO2 Material and Electrodes. *Appl. Surf. Sci.* **2021**, *535*, No. 147699.
- (56) Leinen, D.; Fernández, A.; Espinós, J.; González-Elipe, A. XPS and ISS Study of NiTiO3 and PbTiO3 Subjected to Low-Energy Ion Bombardment. I. Influence of the Type of Ion (Ar+ and O). *Surf. Interface Anal.* 1993, 20, 941–948.
- (57) Kim, J.-N.; Shin, K.-S.; Kim, D.-H.; Park, B.-O.; Kim, N.-K.; Cho, S.-H. Changes in Chemical Behavior of Thin Film Lead Zirconate Titanate During Ar+-ion Bombardment using XPS. *Appl. Surf. Sci.* **2003**, *206*, 119–128.
- (58) Panzner, G.; Egert, B.; Schmidt, H. P. The Stability of CuO and Cu2O Surfaces During Argon Sputtering Studied by XPS and AES. *Surf. Sci.* **1985**, *151*, 400–408.
- (59) Cherkashinin, G.; Nikolowski, K.; Ehrenberg, H.; Jacke, S.; Dimesso, L.; Jaegermann, W. The Stability of the SEI Layer, Surface Composition and the Oxidation State of Transition Metals at the Electrolyte—Cathode Interface Impacted by the Electrochemical Cycling: X-Ray Photoelectron Spectroscopy Investigation. *Phys. Chem. Chem. Phys.* **2012**, *14*, 12321—12331.
- (60) Li, D.; Li, H.; Danilov, D.; Gao, L.; Zhou, J.; Eichel, R.-A.; Yang, Y.; Notten, P. H. L. Temperature-Dependent Cycling Performance and Ageing Mechanisms Of C6/LiNi1/3Mn1/3Co1/3O2 Batteries. *J. Power Sources* **2018**, *396*, 444–452.
- (61) Hekmatfar, M.; Hasa, I.; Eghbal, R.; Carvalho, D. V.; Moretti, A.; Passerini, S. Effect of Electrolyte Additives on the LiNi0.5Mn0.3-Co0.2O2 Surface Film Formation with Lithium and Graphite Negative Electrodes. *Adv. Mater. Interfaces* **2020**, 7, No. 1901500.
- (62) Kosova, N. V.; Devyatkina, E. T.; Kaichev, V. V.; Kellerman, D. G. Effect of Electronic State of Ions on the Electrochemical Properties of Layered Cathode Materials LiNi_{1-2x}Co_xMn_xO₂. *Russ. J. Electrochem.* **2008**, *44*, 543–549.
- (63) Shaju, K. M.; Bruce, P. G. Macroporous Li(Ni1/3Co1/3Mn1/3)O2: A High-Power and High-Energy Cathode for Rechargeable Lithium Batteries. *Adv. Mater.* **2006**, *18*, 2330–2334.
- (64) Källquist, I.; Martin, J.-F.; Naylor, A. J.; Baur, C.; Fichtner, M.; Colin, J.-F.; Brandell, D.; Edström, K.; Hahlin, M. Influence of Electrolyte Additives on the Degradation of Li2VO2F Li-Rich Cathodes. *J. Phys. Chem. C* **2020**, *124*, 12956–12967.
- (65) Cappel, U. B.; Liu, P.; Johansson, F. O.; Philippe, B.; Giangrisostomi, E.; Ovsyannikov, R.; Lindblad, A.; Kloo, L.; Gardner, J. M.; Rensmo, H. Electronic Structure Characterization of Cross-Linked Sulfur Polymers. *ChemPhysChem* **2018**, *19*, 1041–1047.
- (66) Yu, L.; Takagi, Y.; Nakamura, T.; Sakata, T.; Uruga, T.; Tada, M.; Iwasawa, Y.; Masaoka, S.; Yokoyama, T. Operando Observation of Sulfur Species Poisoning Polymer Electrolyte Fuel Cell Studied by Near Ambient Pressure Hard X-ray Photoelectron Spectroscopy. *J. Phys. Chem. C* **2019**, *123*, 603–611.
- (67) Doubaji, S.; Philippe, B.; Saadoune, I.; Gorgoi, M.; Gustafsson, T.; Solhy, A.; Valvo, M.; Rensmo, H.; Edström, K. Passivation Layer and Cathodic Redox Reactions in Sodium-Ion Batteries Probed by HAXPES. *ChemSusChem* **2016**, *9*, 97–108.
- (68) Liu, H.; Naylor, A. J.; Menon, A. S.; Brant, W. R.; Edström, K.; Younesi, R. Understanding the Roles of Tris(trimethylsilyl) Phosphite (TMSPi) in LiNi0.8Mn0.1Co0.1O2 (NMC811)/Silicon—Graphite (Si–Gr) Lithium-Ion Batteries. *Adv. Mater. Interfaces* **2020**, 7, No. 2000277.
- (69) Björklund, E.; Naylor, A. J.; Brant, W.; Brandell, D.; Younesi, R.; Edström, K. Temperature Dependence of Electrochemical Degradation in LiNi1/3Mn1/3Co1/3O2/Li4Ti5O12 Cells. *Energy Technol.* **2019**, *7*, No. 1900310.
- (70) Gu, M.; Belharouak, I.; Zheng, J.; Wu, H.; Xiao, J.; Genc, A.; Amine, K.; Thevuthasan, S.; Baer, D. R.; Zhang, J.-G.; et al. Formation of the Spinel Phase in the Layered Composite Cathode used in Li-Ion Batteries. *ACS Nano* **2013**, *7*, 760–767.
- (71) Hwang, S.; Kim, S. M.; Bak, S.-M.; Chung, K. Y.; Chang, W. Investigating the Reversibility of Structural Modifications of LixNiyMnzCo1-y-zO2 Cathode Materials during Initial Charge/Discharge, at Multiple Length Scales. *Chem. Mater.* **2015**, 27, 6044–6052.

- (72) Jung, S.-K.; Gwon, H.; Hong, J.; Park, K.-Y.; Seo, D.-H.; Kim, H.; Hyun, J.; Yang, W.; Kang, K. Understanding the Degradation Mechanisms of LiNi0.5Co0.2Mn0.3O2 Cathode Material in Lithium Ion Batteries. *Adv. Energy Mater.* **2014**, *4*, No. 1300787.
- (73) Shui Zhang, S. An Unique Lithium Salt for the Improved Electrolyte Of Li-Ion Battery. *Electrochem. Commun.* **2006**, *8*, 1423–1428.
- (74) Shkrob, I. A.; Wishart, J. F.; Abraham, D. P. What Makes Fluoroethylene Carbonate Different? *J. Phys. Chem. C* **2015**, *119*, 14954–14964.
- (75) Markevich, E.; Salitra, G.; Aurbach, D. Fluoroethylene Carbonate as an Important Component for the Formation of an Effective Solid Electrolyte Interphase on Anodes and Cathodes for Advanced Li-Ion Batteries. ACS Energy Lett. 2017, 2, 1337–1345.

□ Recommended by ACS

Onset Potential for Electrolyte Oxidation and Ni-Rich Cathode Degradation in Lithium-Ion Batteries

Wesley M. Dose, Clare P. Grey, et al.

SEPTEMBER 22, 2022 ACS ENERGY LETTERS

READ 🗹

A Nearly Zero-Strain Li-Rich Rock-Salt Oxide with Multielectron Redox Reactions as a Cathode for Li-Ion Batteries

Ke Zhou, Yong Yang, et al.

OCTOBER 19, 2022

CHEMISTRY OF MATERIALS

READ 🗹

Unraveling the State of Charge-Dependent Electronic and Ionic Structure-Property Relationships in NCM622 Cells by Multiscale Characterization

Albina Jetybayeva, Seungbum Hong, et al.

JANUARY 24, 2022

ACS APPLIED ENERGY MATERIALS

READ **C**

Enhancing the Electrochemical Performance of Olivine $LiMnPO_4$ as Cathode Materials for Li-Ion Batteries by Ni–Fe Codoping

Said Oukahou, Abdellatif Hasnaoui, et al.

SEPTEMBER 09, 2022

ACS APPLIED ENERGY MATERIALS

READ 🗹

Get More Suggestions >